are presently studying analogous lanthanide iodide phases containing both 3d and 5d interstitials that also contain antiprismatic chains.

Acknowledgment. The magnetic data were obtained through the cooperation of J. E. Ostenson. This research was supported by the National Science Foundation, Solid State Chemistry, via Grant DMR-8902954 and was carried out in facilities of the Ames Laboratory, DOE.

Supplementary Material Available: Tables of crystal and refinement data and of anisotropic atom displacement parameters for Y_4I_4Os and the Curie–Weiss plot of the susceptibility of Er_4Br_4Os (Figure 4) (3 pages); a table of observed and calculated structure factor data for Y_4I_4Os (5 pages). Ordering information is given on any current masthead page.

Models of Heme d_1. Molecular Structure and NMR Characterization of an Iron(III) Dioxoisobacteriochlorin (Porphyrindione)

K. M. Barkigia,*[1a] C. K. Chang,[1b] J. Fajer,[1a] and M. W. Renner*[1a]

Contribution from the Department of Applied Science, Brookhaven National Laboratory, Upton, New York 11973, and Department of Chemistry, Michigan State University, East Lansing, Michigan 48824. *Received August 8, 1991*

Abstract: Crystallographic and NMR results are reported for **4**, the $ClFe^{III}$ complex of 2,7-dioxo-3,3′,8,8′,12,13,17,18-octaethylporphyrin (**3**). **4** serves as a model for heme d_1, the unusual dioxoisobacteriochlorin (iBC = isobacteriochlorin) prosthetic group of bacterial dissimilatory nitrite reductases. The coordination and displacement of the Fe in **4** are similar to those found in pentacoordinate, high-spin iron(III) porphyrins, as is the domed conformation of its macrocycle. The major differences are the distinct elongation of the Fe–N distances to the saturated pyrroline rings, 2.118 (6) and 2.113 (6) Å, vs those to the pyrrole rings, 2.047 (6) and 2.033 (6) Å. The shorter Cα–Cβ pyrroline bonds bearing the keto groups vs those without the oxygens suggest that the keto groups are in conjugation with the macrocycle π system. These structural data thus provide a rationale for the most distinctive feature between iBCs and dioxo-iBCs: the large differences in Fe and macrocycle redox potentials. In contrast to the influence of the keto groups on the redox and pyrroline structural properties of **4**, NMR data, particularly at the meso positions, are comparable to those recently reported for $ClFe^{III}$OEiBC (Sullivan et al. *J. Am. Chem. Soc.* **1991**, *113*, 5264). Iterative extended Hückel calculations for the HOMOs and LUMOs of **4** correctly predict the effects of the keto groups on the redox properties of the macrocycle. Crystallographic results for the free base **3**, although at poorer precision than for **4**, indicate that the NH protons are localized on adjacent pyrrole rings and that the macrocycle is not inherently ruffled to any significant extent. Crystallographic data for **4**: space group $P\bar{1}$, $a = 11.635$ (3) Å, $b = 16.189$ (5) Å, $c = 9.003$ (5) Å, $\alpha = 96.93$ (3)°, $\beta = 95.92$ (3)°, $\gamma = 93.75$ (2)°, $V = 1669.2$ Å^3, $Z = 2$. The structure was refined against 2421 data points with $F_o > 2\sigma F_o$ to $R_F = 0.065$ and $R_{wF} = 0.064$.

Introduction

The crucial roles of chlorophylls and bacteriochlorophylls in light harvesting and energy conversion in photosynthesis have long focused attention on the physical, chemical, and structural properties of these chromophores.[2] However, an increasing body of evidence indicates that the generic class of hydroporphyrins, porphyrins in which one or more β–β pyrrole bonds are saturated, mediates a wide range of biological functions in addition to photosynthetic reactions. Among the "green" hemes that catalyze biological reactions as diverse as assimilatory and dissimilatory nitrite reductions,[3,4] sulfite reductions,[3] and catalase activity,[5,6] is heme d_1, the iron isobacteriochlorin (iBC)[7] prosthetic group of bacterial dissimilatory nitrite reductases. Heme d_1 is deduced to consist of an unusual dioxoisobacteriochlorin[7] (**1**).

Two salient features of hydroporphyrins have emerged from recent theoretical, experimental, and structural studies of chlorins, bacteriochlorins, and isobacteriochlorins. First, saturation of one or more β–β pyrrole bonds of porphyrins causes shifts of the lowest unoccupied (LUMOs) and highest occupied (HOMOs) molecular orbitals[8] with the results that reduction and oxidation potentials as well as optical spectra are altered.[8-10] Second, the increased saturation of the hydroporphyrins renders them more flexible,[11-15]

(1) (a) Brookhaven National Laboratory. (b) Michigan State University.
(2) For examples, see: *Chlorophylls*, Scheer, H., Ed.; CRC Press, Boca Raton, FL, 1991. *Reaction Centers of Photosynthetic Bacteria*; Michel-Beyerle, M. E., Ed.; Springer-Verlag: Berlin, 1990.
(3) Siegel, L. M.; Murphy, M. J.; Kamin, H. *J. Biol. Chem.* **1973**, *248*, 251. Murphy, M. J.; Siegel, L. M.; Kamin, H. *Ibid.* **1973**, *248*, 2801. Murphy, M. J.; Siegel, L. M.; Tove, S. R.; Kamin, H. *Proc. Natl. Acad. Sci. U.S.A.* **1974**, *74*, 6121. Vega, J. M.; Garret, R. H. *J. Biol. Chem.* **1975**, *250*, 7980. Ostrowski, J.; Wu, J. Y.; Rueger, D. C.; Miller, B. E.; Siegel, L. M.; Kredich, N. M. *J. Biol. Chem.* **1989**, *264*, 15726.
(4) Horie, S.; Watanabe, T.; Nakamura, S. *J. Biochem.* **1976**, *80*, 579. Kim, C. H.; Hollocher, T. C. *J. Biol. Chem.* **1983**, *258*, 4861.
(5) Jacob, G. S.; Orme-Johnson, W. H. *J. Biol. Chem.* **1979**, *18*, 2967.
(6) Chiu, J. T.; Loewen, P. C.; Switala, J.; Gennis, R. B.; Timkovich, R. *J. Am. Chem. Soc.* **1989**, *111*, 7046.
(7) Chang, C. K.; Timkovitch, R.; Wu, W. *Biochemistry* **1986**, *25*, 8447. Wu, W.; Chang, C. K. *J. Am. Chem. Soc.* **1987**, *109*, 3149. Chang, C. K.; Wu, W. *J. Biol. Chem.* **1986**, *261*, 8593. Weeg-Aerssens, E.; Wu, W.; Ye, R. W.; Tiedje, J. M.; Chang, C. K. *J. Biol. Chem.* **1991**, *266*, 7496.
(8) Chang, C. K.; Hanson, L. K.; Richardson, P. F.; Young, R.; Fajer, J. *Proc. Natl. Acad. Sci. U.S.A.* **1981**, *78*, 2652.
(9) Stolzenberg, A. M.; Spreer, L. O.; Holm, R. H. *J. Am. Chem. Soc.* **1980**, *102*, 364. Stolzenberg, A. M.; Strauss, S. H.; Holm, R. H. *J. Am. Chem. Soc.* **1981**, *103*, 4763.
(10) Richardson, P. F.; Chang, C. K.; Hanson, L. K.; Spaulding, L. D.; Fajer, J. *J. Phys. Chem.* **1979**, *83*, 3420. Richardson, P. F.; Chang, C. K.; Spaulding, L. D.; Fajer, J. *J. Am. Chem. Soc.* **1979**, *101*, 7736. Chang, C. K.; Fajer, J. *J. Am. Chem. Soc.* **1980**, *102*, 848. Fujita, E.; Chang, C. K.; Fajer, J. *J. Am. Chem. Soc.* **1985**, *107*, 7665.
(11) Eschenmoser, A. *Ann. N.Y. Acad. Sci.* **1986**, *471*, 108. Kratky, C.; Waditschatka, R.; Angst, C.; Johansen, J. E.; Plaquevent, J. C.; Schreiberg, J.; Eschenmoser, A. *Helv. Chim. Acta* **1985**, *68*, 1312 and references therein.

0002-7863/92/1514-1701$03.00/0

thereby allowing further modulation of the HOMOs and LUMOs[16] and also providing a structural mechanism for accommodation of different spin and redox states of the metals complexed by the macrocycles.[11,12,15] Indeed, the ruffled conformation of a Ni(II)–dioxo-iBC model of heme d_1 (**2**) led Montforts et al.[17] to raise the possibility that its "saddle-shaped structure is responsible for the biological function of heme d_1". However, nickel(II) hydroporphyrins are well-known to assume ruffled shapes to satisfy the tendency for short Ni(II)–N distances,[11,12,14,15] and a Cu(II) dioxo iBC (**5**) structure clearly shows its macrocycle to be nearly planar.[18]

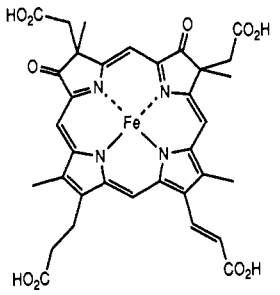

1

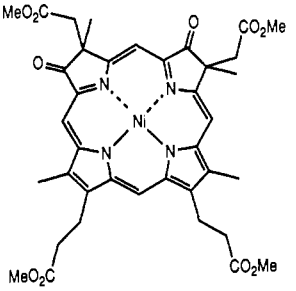

2

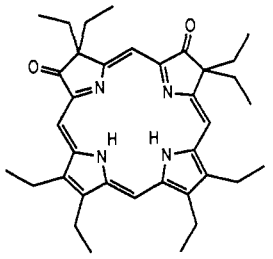

3
4 = Fe(III)Cl
5 = Cu(II)

We present here crystallographic determinations of the metal-free ligand (**3**) and of its iron(III) chloride derivative (**4**) in order to better model heme d_1 and the structural properties of the dioxo-iBC macrocycle. The conformation of the Fe(III) complex is quite normal and closely resembles those of high-spin iron(III) porphyrins.[19] However, in the structures of **3**–**5**, the two keto groups appear to be in conjugation with the iBC π system and thereby *minimize* the distinctive characteristics of iBCs, which are normally harder to reduce and easier to oxidize than porphyrins.[8-10] The introduction of the electronegative keto groups thus causes the dioxo-iBC macrocycle to be *easier* to reduce and *harder* to oxidize than an iBC lacking such functional groups.[18,20]

Table I. Crystallographic Details for **3** and **4**

	3	4
formula	$C_{36}N_4O_2H_{46}$	$FeClC_{36}N_4O_2H_{44}$
MW	566.79	656.07
crystallized from	methyl isobutyl ketone–ethyl acetate	EtOH–$C_2H_4Cl_2$
space group	$C2/c$	$P\bar{1}$
Z	8	2
a, Å	30.799 (10)	11.635 (3)
b, Å	20.806 (19)	16.189 (5)
c, Å	13.275 (7)	9.003 (5)
α, deg	90.0	96.93 (3)
β, deg	103.96 (4)	95.92 (3)
γ, deg	90.0	93.75 (2)
V, Å^3	8255.4	1669.2
crystal size	0.45 × 0.60 × 0.60 mm	0.20 × 0.40 × 0.08 mm
2θ range, deg	4–40	4–45
data measured	$\pm h,\pm k,+l$	$h,\pm k,\pm l$
no. measured	13 186	5016
no. unique data	3995	4102
structure solution	MULTAN 78	SHELXS-86
refinement	2460 data with $F_o > 3\sigma F_o$	2421 with $F_o > 2\sigma F_o$
R_F	0.102	0.065
R_{wF}	0.156	0.064
T, K	298	200

(Chang and Wu[7] have suggested the name "porphyrindione" to emphasize the role of the keto groups.) NMR results for the Fe(III) complex help to characterize the electronic configuration of the compound. In marked contrast to the significant effects of the dioxo groups on the redox properties of the metal and the macrocycle,[18] the NMR spectrum of **4** is surprisingly similar to that of ClFe^{III}OEiBC (**6**).[21]

Although the poor quality of the crystal of **3** resulted in high R values, the results are sufficiently reliable to establish that the conformation of the metal-free ligand is similar to that of the Cu(II) derivative;[18] i.e., the dioxo macrocycle is not inherently ruffled to any large extent. In addition, the crystallographic results clearly demonstrate that the NH protons are localized on adjacent pyrrole rings as shown for the structural formula of **3**.

Methods

Free-base dioxo-iBC **3** (2,7-dioxo-3,3′,8,8′,12,13,17,18-octaethylporphyrin) was obtained as previously described.[22,23] Iron was inserted into **3** by the standard ferrous sulfate–pyridine–acetic acid method.[24] Optical maxima for **4** (nm) ($\epsilon \times 10^{-3}$) in CH_2Cl_2: 755 (2.36), 672 (2.75), 611 (12.4), 579 (9.7), 525 (9.58), 403 (37.0), 376 (45.0).

For NMR experiments, the meso positions of **3** were selectively deuterated with D_2SO_4–D_2O using the method of Stolzenberg and Laliberte.[25] The meso d_4 derivative was prepared from octaethylporphyrin-d_4 using the rearrangement synthesis for **3**.[26] The sites and percentage of deuteration were established by ^{1}H NMR. Iron was then inserted as above. The iron(III) iodide analogue of **4** was synthesized via metathesis reaction of the chloride salt using KI in toluene–water. NMR solvents were purified and dried using standard techniques. NMR spectra were recorded on a Bruker AM300 spectrometer operating at 300.13 MHz for ^{1}H and 46.07 MHz for ^{2}H and coupled to a Aspect 3000 computer. Chemical shifts are referenced against TMS.

Iterative extended Hückel (IEH) calculations for **4** used the crystallographic coordinates reported here. The programs are described in ref 8.

Crystallographic data were collected on an Enraf-Nonius CAD4 diffractometer with graphite-monochromated Mo Kα radiation, λ = 0.7107 Å. Details are given in Table I. Both structures were corrected for absorption by the analytical method using the CRYSNET series of programs.[27] Scattering factors were taken from standard compilations.[28]

(12) Strauss, S. H.; Silver, M. E.; Long, K. M.; Thompson, R. G.; Hudgens, R. A.; Spartalian, K.; Ibers, J. A. *J. Am. Chem. Soc.* **1985**, *107*, 4207. Suh, M. P.; Swepston, P. N.; Ibers, J. A. *J. Am. Chem. Soc.* **1984**, *106*, 5164.
(13) Barkigia, K. M.; Gottfried, D. S.; Boxer, S. G.; Fajer, J. *J. Am. Chem. Soc.* **1989**, *111*, 6444. Barkigia, K. M.; Fajer, J.; Chang, C. K.; Williams, G. J. B. *J. Am. Chem. Soc.* **1982**, *104*, 315. Barkigia, K. M.; Chantranupong, L.; Smith, K. M.; Fajer, J. *J. Am. Chem. Soc.* **1988**, *110*, 7566. Barkigia, K. M.; Chang, C. K.; Fajer, J. *J. Am. Chem. Soc.* **1991**, *113*, 7445.
(14) Stolzenberg, A. M.; Glazer, P. A.; Foxman, B. M. *Inorg. Chem.* **1986**, *25*, 983.
(15) Renner, M. W.; Furenlid, L. R.; Barkigia, K. M.; Forman, A.; Shim, H.-K.; Simpson, D. J.; Smith, K. M.; Fajer, J. *J. Am. Chem. Soc.* **1991**, *113*, 6891.
(16) Gudowska-Nowak, E.; Newton, M. D.; Fajer, J. *J. Phys. Chem.* **1990**, *94*, 5795. Renner, M. W.; Cheng, R. J.; Chang, C. K.; Fajer, J. *J. Phys. Chem.* **1990**, *94*, 8508.
(17) Montforts, F. P.; Romanowski, F.; Bats, J. W. *Angew. Chem., Int. Ed. Engl.* **1989**, *28*, 480.
(18) Chang, C. K.; Barkigia, K. M.; Hanson, L. K.; Fajer, J. *J. Am. Chem. Soc.* **1986**, *108*, 1342.
(19) Scheidt, W. R.; Reed, C. A. *Chem. Rev.* **1981**, *81*, 543. Scheidt, W. R.; Lee, Y. J. *Struct. Bonding (Berlin)* **1987**, *64*, 1.
(20) Similar effects of keto functions are observed in porphyrins and other hydroporphyrins.[15]
(21) Sullivan, E. P.; Grantham, J. D.; Thomas, C. S.; Strauss, S. H. *J. Am. Chem. Soc.* **1991**, *113*, 5264. (OEiBC in this study is 2,3,7,8-tetrahydro-2′,3′,7′,8′,12,13,17,18-octaethylporphyrin.)
(22) Inhoffen, H. H.; Nolte, W. *Liebigs Ann. Chem.* **1969**, *725*, 167.
(23) Chang, C. K. *Biochemistry* **1980**, *19*, 1971.
(24) Chang, C. K.; DiNello, R. K.; Dolphin, D. *Inorg. Synth.* **1980**, *20*, 147.
(25) Stolzenberg, A. M.; Laliberte, M. A. *J. Org. Chem.* **1987**, *52*, 1022.
(26) Chang, C. K.; Sotiriou, C.; Wu, W. *J. Chem. Soc., Chem. Commun.* **1986**, 1213.

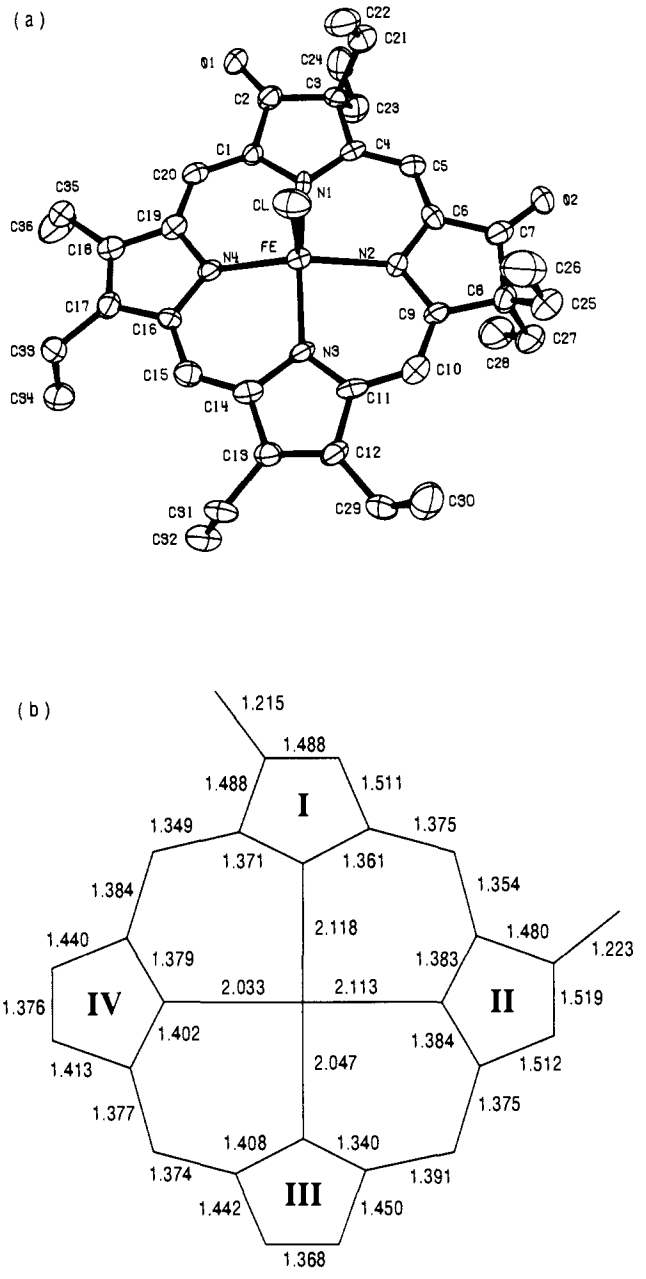

Figure 1. (a) Molecular structure of **4**. Ellipsoids enclose 50% probability. Hydrogens are omitted for clarity. (b) Bond distances for **4** (Å). The average esd of an Fe–N bond is 0.006 Å and that of a typical C–C bond 0.010 Å.

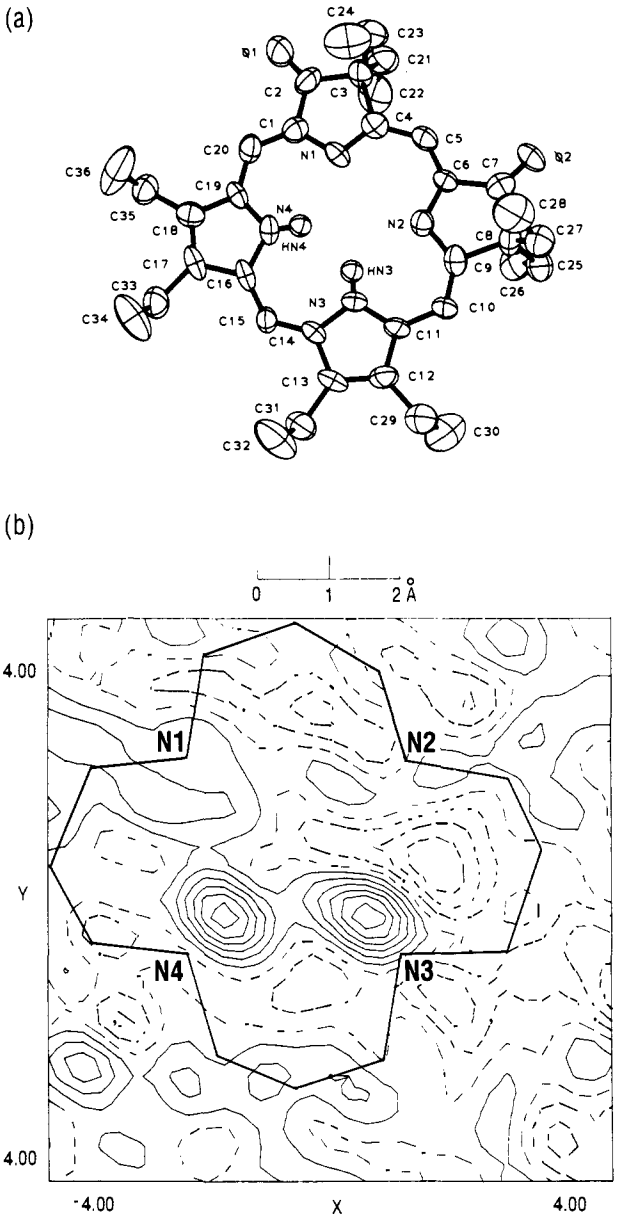

Figure 2. (a) Molecular structure of **3**. Ellipsoids enclose 50% probability except for hydrogens HN3 and HN4, which are not to scale. All other hydrogens are omitted for clarity. (b) Difference electron density map calculated[27b] in the plane of the nitrogens of **3**. The contour intervals are shown in units of 0.05 e/Å^3 with negative density indicated by broken lines. The heavy line traces the nitrogens and the α- and meso-carbons. The map establishes that the NH hydrogens are localized on N3 and N4.

The structures of **4** and **3** were solved using SHELXS-86[29] and MULTAN 78,[30] respectively. The hydrogens in **3** were placed in calculated positions, except for those on the nitrogens which were experimentally determined. Most of the hydrogens in **4** were located in difference Fourier maps and were subsequently idealized. Both structures were refined by full-matrix least squares with anisotropic thermal parameters for all non-hydrogen atoms. Due to the poor crystal quality of **3**, its R factor is considerably worse than that of the Fe complex **4**. Nonetheless, the results for **3** are included to illustrate the consequences of demetalating the complex.

Results and Discussion

1. Crystallography. The molecular structures of **4** and **3** are presented in Figures 1a and 2a, respectively. Bond distances in **4** are given in Figure 1b. Deviations from planarity for **4** are shown in Figure 3, which also offers a graphic display of the deviations of the 24-atom core from the plane of the four nitrogens. Final positional parameters for the non-hydrogen atoms of **4** and **3** are included in the supplementary material.

As expected[11-15,17,18] from the saturation of the Cβ–Cβ bonds in the pyrroline rings I and II, those bonds are elongated and average 1.504 (10) and 1.520 (13) Å in **4** and **3**, respectively. The Cα–Cβ bonds in those rings are lengthened as well. The average Cβ–O distances of 1.219 (9) and 1.207 (11) Å in **4** and **3** are diagnostic of keto functions. The effects of the oxygens are reflected in the Cα–Cβ bonds to which they are attached. These

(27) (a) Berman, H. M., Bernstein, F. C., Bernstein, H. J., Koetzle, T. F., Williams, G. J. B., Eds. Informal Report, BNL 21714, Brookhaven National Laboratory, Upton, NY, 1976. (b) Figure 2b was generated with a local version of NIELSAV which uses the slant plane Fourier transform algorithm of van de Waal, B. W., SPFT, Twente University of Technology, Enschede, The Netherlands, 1975.

(28) Scattering factors for non-hydrogen atoms are taken from: Cromer, D. T.; Mann, J. B. *Acta Crystallogr., Sect. A* **1968**, *A24*, 321. Scattering factors for hydrogens are from: Stewart, R. F.; Davidson, E. R.; Simpson, W. T. *J. Chem. Phys.* **1965**, *42*, 3172.

(29) Sheldrick, G. M. *Crystallographic Computing 3*; Sheldrick, G. M., Kurger, C., Goddard, R., Eds.; Oxford University Press: Oxford, 1985; p 175.

(30) Main, P.; Hill, S. E.; Lessinger, L.; Germain, G.; Declercq, J. P.; Woolfson, M. M.; MULTAN 78, A System of Computer Programs for the Automatic Solution of Crystal Structures from X-ray Diffraction Data, University of York, England, and University of Louvain, Belgium, 1978.

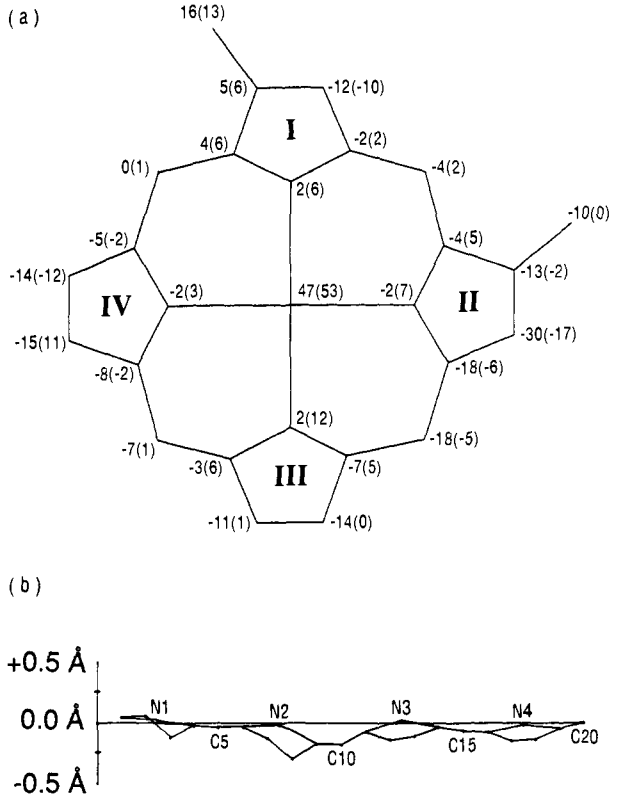

Figure 3. (a) Displacements of the core atoms of **4** from the plane defined by the four nitrogens and, in parentheses, from the plane of the 24-atom core, in units of 0.01 Å. (b) Linear displacements of the core atoms of **4** from the nitrogen plane that illustrate the doming of the macrocycle. The horizontal axis is not to scale.

are significantly shorter than the corresponding Cα–Cβ bonds in the pyrroline rings bearing the ethyl groups: 1.484 (10) vs 1.512 (10) Å in **4** and 1.483 (13) vs 1.541 (13) Å in **3**. A similar trend was observed[18] in the Cu(II) derivative **5**: 1.473 (8) vs 1.517 (8) Å. These results suggest therefore that the keto groups in **3**–**5** are in conjugation with the π systems of the macrocycles and, consequently, affect their electronic properties (vide infra). (We have observed[31] similar effects in chlorins and bacteriochlorins bearing exocyclic double bonds on the pyrroline Cβ positions.)

As observed in other hydroporphyrins,[11-15,17,19,32] the metal to nitrogen distances in **4** are longer to the pyrroline rings than to the pyrroles: Fe–N1 = 2.118 (6) and Fe–N2 = 2.113 (6) Å vs Fe–N3 = 2.047 (6) and Fe–N4 = 2.033 (6) Å. For comparison, Fe–N distances with mean values of 2.065 Å are typically found in high-spin, pentacoordinate iron(III) porphyrins.[19]

The longer Fe–N bonds to rings I and II in **4** derive, at least in part, from the wider Cα–N–Cα bond angles, which result in turn from the elongated Cβ–Cβ bonds in the pyrroline rings. The Cα–N–Cα angles average 108.7 (6)° in rings I and II and 104.7 (6)° in pyrrole rings III and IV. This characteristic angle difference in metallohydroporphyrins is masked in **3**. The Cα–N–Cα angles in the saturated rings are again wide, 110.2 (8)°, but those in the pyrrole rings average 111.3 (8)°. The latter effect is common to protonated pyrrole rings,[33] and indeed, the hydrogens on N3 and N4 were located in a difference Fourier map (Figure 2b). The crystallographic results thus confirm the conclusion, reached on the basis of NMR data,[7] that the NH protons in **3** are localized on the two adjacent pyrrole rings.

The different hybridizations of the Cβ atoms bearing the keto groups vs those bearing the two ethyl groups in rings I and II result in asymmetries in the Cα–Cβ–Cβ angles which open to 106.6 (5)° at C2 and C7 in **4** and to 107.0 (8)° in **3** to be compared to 101.5 (6)° and 100,5 (8)° at C3 and C8 of **4** and **3**, respectively. This effect is further manifested in the Cα–Cβ–O and Cβ–Cβ–O angles which average 126.7 (6)° and 126.5 (10)° in **4** and **3**, respectively, in contrast to the more tetrahedral Cα–Cβ–C_{Et} and Cβ–Cβ–C_{Et} angles which average 110.7 (4)° and 111.8 (6)° in **4** and **3**, respectively.

The conformation and deviations from planarity for **4** are illustrated in Figure 3. Those for **3** are included in the supplementary material.

The nitrogens lie in a plane within 0.02 Å in **4** and 0.01 Å in **3**. The largest displacements of the core atoms from the plane of the nitrogens occur at C8 of **4**, 0.30 Å, and at C15 of **3**, 0.13 Å. The Fe sits 0.47 Å above the plane of the nitrogens and 0.53 Å above the 24-atom plane. These values are *typical* of high-spin, pentacoordinate iron(III) porphyrins[19] which exhibit comparable mean values of 0.47 and 0.51 Å. The Fe–Cl distance of 2.218 (3) Å is identical to that found in chlorohemin,[34] 2.218 (6) Å, and similar to that in $ClFe^{III}$(tetraphenylporphyrin),[35] 2.192 (12) Å. The coordination of the Cl is irregular; the N–Fe–Cl angles range from 97.2 (2) to 107.2 (2)°, with the Cl pointing toward ring I. The similarity between the Fe coordination in **4** and that of porphyrins parallels that observed between (μ-O)(Fe^{III}(tetraphenylporphyrin) and chlorin)$_2$. Strauss et al.[32] noted that the Fe–O–Fe angles, Fe–O distances, and Fe out-of-plane displacements are "virtually the same for the two compounds".

4 is domed with all the Cβ atoms except C2 lying below the plane of the nitrogens (Figure 3b). This conformation is again common to pentacoordinate iron(III) porphyrins.[19,33] In contrast, **3** assumes an S_4 configuration, with adjacent rings alternately directed up and down. The deviations from planarity are not large, however, ≤0.13 Å, and are comparable to those found in **5**.[18] Indeed, the conformations and orientations of substituents in **3** and **5** are nearly identical.

The increasing interest in green hemes and their biological roles has prompted several resonance Raman studies of hydroporphyrins and of the effects of their structural variations on vibrational assignments.[36-38] In agreement with the conclusions reached above that the keto groups of **3**–**5** are in conjugation with the π systems of the macrocycles, excitation in the visible absorption bands of **5** yields diagnostic *RR* keto marker bands.[36] Core markers have also elicited particular attention. The structures of **3**–**5** offer some insight into the effects of metal incorporation and coordination on the core parameters Ct–N and Ct–Cα. For the Fe, Cu, and H_2 derivatives, respectively, average Ct–N values are 2.024 (7), 2.022 (7), and 2.095 (4) Å and Ct–Cα values are 3.052 (7), 3.046 (6), and 3.083 (24) Å. In spite of their different conformations, the parameters of the metallo complexes are thus quite similar while those of the free base are larger, even with the caveat that the results for the latter are less precise. Hoard[33] has noted similar differences in Ct–N between free base and copper(II) *meso*-tetrapropylporphyrins. Additional comparisons of bond distances and angles for **3**–**5** are presented in Table II.

The molecules of **4** pack as dimers with the monomer subunits centrosymmetrically related. In the dimers with the concave sides of the domed macrocycles facing each other, and the chlorines pointing away from each other, there are no contacts smaller than 4 Å between atoms of the two subunits and the Fe–Fe distances are 7.72 Å. There are contacts as short as 3.36 Å between other inversion-related molecules whose Cl atoms face toward each other, but the Fe–Fe distances are longer, 7.94 Å. In neither case are there distances between pyrrole or pyrroline centers shorter than 4.5 Å.

(31) Barkigia, K. M.; Thompson, M. A.; Pandey, R. K.; Smith, K. M.; Vicente, M. G. H.; Fajer, J. *New J. Chem.*, in press. Barkigia, K. M.; Fajer, J.; Chang, C. K.; Young, R. *J. Am. Chem. Soc.* **1984**, *106*, 6457.
(32) Strauss, S. H.; Pawlik, M. J.; Skowyra, J.; Kennedy, J. R.; Anderson, O. P.; Spartalian, K.; Dye, J. L. *Inorg. Chem.* **1987**, *26*, 724.
(33) Hoard, J. L. *Porphyrins and Metalloporphyrins*; Smith, K. M., Ed.; Elsevier: Amsterdam, 1975; p 317.
(34) Koenig, D. F. *Acta Crystallogr.* **1965**, *18*, 663.
(35) Hoard, J. L.; Cohen, G. H.; Glick, M. D. *J. Am. Chem. Soc.* **1967**, *89*, 1992.
(36) Mylrajan, M.; Anderson, L. A.; Loehr, T. M.; Wu, W.; Chang, C. K. *J. Am. Chem. Soc.* **1991**, *113*, 5000.
(37) Procyk, A. D.; Bocian, D. F. *J. Am. Chem. Soc.* **1991**, *113*, 3765.
(38) Melamed, D.; Sullivan, E. P.; Prendergast, K.; Strauss, S. H.; Spiro, T. G. *Inorg. Chem.* **1991**, *30*, 1308.

Table II. Comparison of Selected Distances (Å) and Angles (deg) in **3–5**[a]

	4	3	5
M–N_{sat}	2.116 (6)		2.044 (5)
M–N_{uns}	2.040 (6)		1.999 (5)
Cα–Cβ(O)	1.484 (10)	1.483 (13)	1.473 (8)
Cα–Cβ(Et_2)	1.512 (10)	1.541 (13)	1.517 (8)
Cα–$Cβ_{uns}$	1.436 (8)	1.417 (13)	1.442 (6)
Cβ–$Cβ_{sat}$	1.504 (10)	1.520 (13)	1.515 (8)
Cβ–$Cβ_{uns}$	1.372 (10)	1.381 (13)	1.362 (8)
N–Cα	1.379 (8)	1.369 (8)	1.375 (5)
Cα–Cm	1.372 (5)	1.370 (11)	1.369 (7)
Cβ–O	1.219 (9)	1.207 (11)	1.216 (8)
Ct–C5	3.396 (11)	3.308 (14)	3.377 (7)
Ct–C10, C20	3.392 (10)	3.518 (10)	3.406 (7)
Ct–C15	3.425 (11)	3.337 (13)	3.405 (7)
Ct–$Cm_{(av)}$	3.401 (9)	3.420 (57)	3.398 (7)
Ct–$Cα_{sat}$	3.042 (9)	3.076 (39)	3.038 (11)
Ct–$Cα_{uns}$	3.063 (10)	3.089 (39)	3.053 (3)
Ct–$Cα_{(av)}$	3.052 (7)	3.083 (24)	3.046 (6)
N–M–N_{adj}	87.1 (6)		90.0 (4)
N–M–N_{opp}	153.9 (2)		178.7 (3)
M–N–Cα	126.1 (7)		126.4 (6)
Cm–Cα–$Cβ_{sat}$	123.0 (11)	122.9 (4)	122.5 (3)
Cm–Cα–$Cβ_{uns}$	127.6 (4)	125.2 (7)	125.3 (1)
N–Cα–Cm	124.7 (6)	126.2 (6)	125.0 (5)
Cα–Cm–Cα	127.4 (4)	128.4 (13)	127.0 (1)
Cα–Cβ–Cβ(Et_2)	106.6 (5)	107.0 (8)	106.7 (5)
Cα–Cβ–Cβ(O)	101.5 (6)	100.5 (8)	101.0 (5)
N–Cα–$Cβ_{sat}$	111.4 (7)	111.1 (9)	111.7 (7)
N–Cα–$Cβ_{uns}$	111.1 (7)	106.1 (11)	110.5 (4)
Cα–Cβ–O	126.6 (7)	127.5 (10)	127.0 (6)
Cβ–Cα–O	126.9 (7)	125.6 (10)	126.3 (6)
Cα–Cβ–C_{Et}	110.9 (7)	112.9 (5)	113.0 (4)
Cβ–Cβ–C_{Et}	110.5 (5)	110.8 (8)	110.4 (6)
Cα–Cβ–$Cα_{sat}$	108.7 (6)	110.2 (8)	108.9 (4)
Cα–N–$Cα_{uns}$	104.7 (6)	111.3 (8)	105.4 (4)

[a] sat and uns refer to the pyrroline and pyrrole rings, respectively. The esd of the mean was calculated as $[\sum_m(l_m - \bar{l})^2/m(m-1)]^{1/2}$ for more than two contributors and as the average of the esds for two contributors.

The molecules of **3** also form dimers related by centers of symmetry. The center of ring IV is 4.03 Å from its symmetry mate, and the center of ring III is 4.27 Å from inversion-related ring IV. There are individual contacts of 3.38 Å between C15 of one molecule and C19 of its symmetry-related partner. Packing diagrams for **3** and **4** are included in the supplementary material.

2. NMR Results for Fe^{III}X-dioxo-iBC. The use of ^{1}H NMR to characterize the solution properties of iron porphyrins is well documented.[39,40] Such data provide information about the oxidation, spin, and ligation states of the compounds. We extend here the structural characterization of the Fe(III)–dioxo-iBC complex to consider its electronic configuration in solution.

Resonance Assignments. Both chloride and iodide salts of the complex were investigated. Narrowed linewidths are observed for the latter. In pentacoordinate high spin Fe(III) porphyrins,[41] the line widths follow an inverse trend in the zero-field parameter *D*. The same trends holds for **4**: The line widths decrease by a factor of 4 on substitution of I^- for Cl^-. *D* is thus positive and decreases on replacement of I^- by Cl^-.

The ^{1}H NMR spectrum of **4** (X = I^-) is shown in Figure 4. Peak assignments were made by comparison with other iron porphyrins, relative areas, line widths, and selective deuterations. The symmetry of **4** is C_1; therefore, 16 methylene, 8 methyl, and 4 meso proton resonances are expected. The four broad upfield resonances are assigned to the meso protons based on the ^{2}H NMR results obtained for meso-d_4, -d_2 (5, 10), and -d_2 (5, 20) derivatives of **4** with X = Cl^- (Figure 5). The methylene resonances of **4** (X = I^-, Figure 4) are located downfield between 80 and 17 ppm.

(39) LaMar, G. N.; Walker, F. A. *The Porphyrins*; Dolphin, D., Ed.; Academic Press: New York, 1979; Vol. IV, p 61.
(40) Goff, H. M. *Iron Porphyrins*; Lever, A. B. P., Gray, H. B., Eds.; Addison-Wesley: Reading, MA, 1983; Part I, p 237.
(41) LaMar, G. N.; Walker, F. A. *J. Am. Chem. Soc.* **1973**, *95*, 6950.

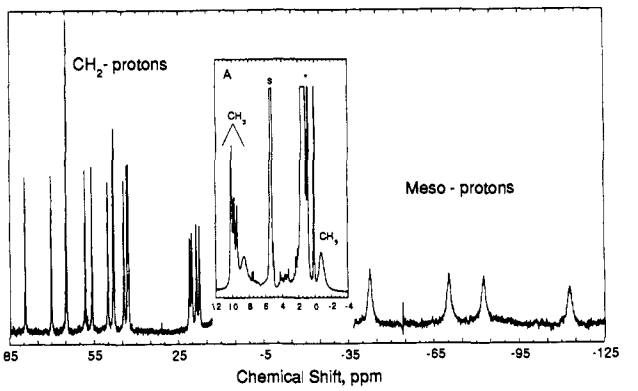

Figure 4. 300-MHz ^{1}H NMR spectrum of **4** (X = I^-) in CD_2Cl_2 at 20 °C.

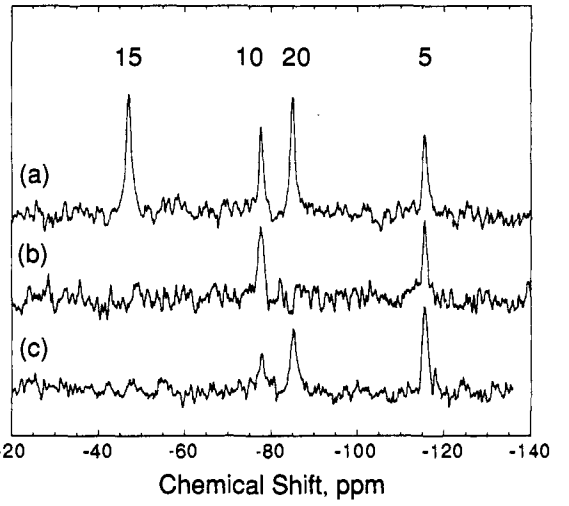

Figure 5. 46-MHz ^{2}H NMR spectra of **4** (X = Cl^-) in CH_2Cl_2 at 20 °C: (a) meso-d_4, (b) meso-d_2 (5, 10), (c) meso-d_2 (5, 20).

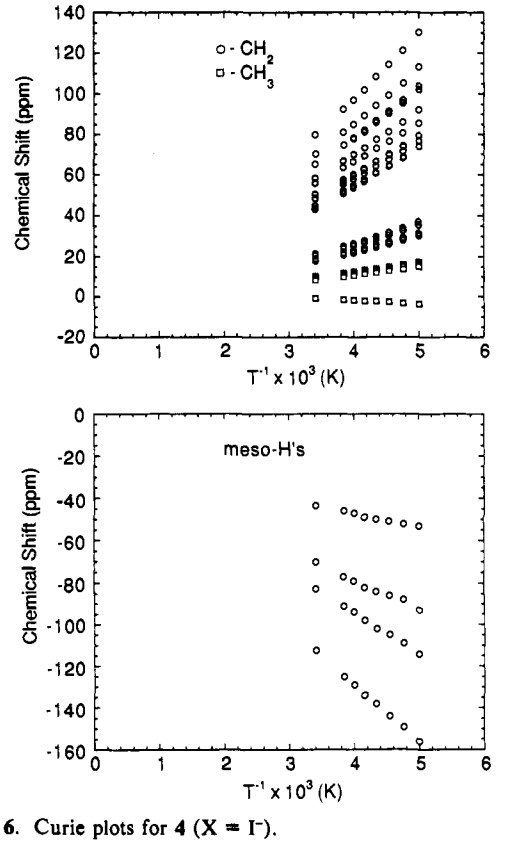

Figure 6. Curie plots for **4** (X = I^-).

Table III. NMR Results for IFe^{III}-dioxo-iBC in CD_2Cl_2

resonance	assignment	4 (X = I⁻)[a]	ClFeOEiBC[b,21]	ClFeOEP[a]
meso H	C15	−44 (448)	−38.4	
	C10	−70 (470)	−77.7	−55 (×4)
	C20	−83 (509)	−77.7	
	C5	−113 (503)	−116.2	
CH_2	pyrroles & pyrrolines	79.7 (51)	pyrroles 70.1	pyrroles 43 (×8)
		70.3 (51)	61.8	39 (×8)
		65.0 (63) (×2)	56.8	
		58.2 (51)	51.7	
		55.8 (59)	40.9	
		50.3 (65)	39.9	
		48.4 (45)	37.6	
		48.2 (51)	34.6	
		44.7 (61)		
		43.4 (59)		
		43.0 (59)		
	pyrrolines	21.3 (92)	pyrrolines 29.7	
		20.5 (93)	27.2	
		18.9 (86)	18.2 (×2)	
		17.8 (88)	14.1 (×2)	
			8.0 (×2)	
CH_3	pyrroles	10.1 (53) (×2)	*c*	pyrroles 6.6 (×24)
		9.8 (47)		
		9.4 (55)		
	pyrrolines	8.7 (280) (×2)		
		−0.73 (210) (×2)		

[a] T = 20 °C. Chemical shifts in ppm (line widths in Hz). [b] T = 25 °C. *ttt* stereoisomer.[21] [c] Not reported.

As expected from the out-of-plane displacement of the Fe observed in the crystal structure of **4**, all the methylene protons in solution should be inequivalent. Indeed, 14 distinct methylene resonances are observed, each equal to one proton, and two are superimposed (peak at 65 ppm). The methyl peaks are located between +11 and −2 ppm. The relative areas of the peaks from left to right in Figure 4 are 2:1:1:2:2 and account for the eight methyl groups. The peak at 10 ppm resolves into two peaks at lower temperatures. Table III presents the chemical shifts and line widths for **4** and a comparison with $ClFe^{III}$OEP (OEP = octaethylporphyrin) and -OEiBC.[21]

For high-spin iron(III) porphyrins, the relaxation mechanism that controls the line widths of the proton resonances is dipolar in origin, giving rise to an r^{-6} line width dependence, where r is the Fe to H distance through space.[39,41] In the crystal structure of **4**, the methylene and methyl groups on the saturated rings are closer to the iron by ≈0.3 and 1 Å, respectively, than those on the pyrrole rings.[42] As shown in Figure 4, four methylene protons and four methyl groups display broader line widths and presumably correspond to the substituents on the saturated rings. However, the spatial orientations of the *gem*-methylene substituents must not be equivalent since only four methylene protons instead of eight are broadened. Note also that all four terminal methyl groups are broadened. (We have observed a similar effect in a monooxoiron(III) chlorin with similar substituents on the pyrroline ring: Only one methylene but both methyl groups are broadened.[43])

Temperature Dependence. High-spin ferric porphyrins exhibit small magnetic anisotropy in which the dipolar shifts contribute less than 10% to the isotropic shifts.[44] The dipolar shifts arise from axial anisotropy due to the sizable zero-field splittings. This results in a slight curvature in the Curie plots due to the T^{-2} component in the dipolar contribution to the isotropic shift. The temperature dependence of **4** in the form of a Curie plot is shown in Figure 6. The chemical shifts versus T^{-1} are not linear, their intercepts at $T^{-1} = 0$ do not correspond to the diamagnetic reference (the Zn(II) complex of **3**), and as in ferric porphyrins, the T^{-2} term must be included. Good fits to the data are obtained using a second-order polynomial.

Electronic Structure. Previous NMR studies of five-coordinate iron(III) hydroporphyrins have documented both the similarities and differences to the analogous porphyrins.[21,45,46] The results for **4** are compared with those for $ClFe^{III}$OEP and OEiBC[21] in Table III. Although the symmetry of **4** is lowered, the general patterns of chemical shifts are retained and are consistent with π spin density at the meso positions and σ spin density at the β positions. (Note the close similarity of the meso proton chemical shifts in **4** and in the OEiBC, **6**.) As evident from the crystallographic results for **4**, saturation of two pyrrole rings leads to elongation of their Fe–N distances and some macrocycle distortion that, in turn, can affect the spin profile. Similar results have been reported for $[Fe^{III}Cl(N\text{-MeOEP})]Cl$, a ferric porphyrin in which the symmetry is also lower, the alkylated pyrrole ring is tilted, and the distance from its N to the Fe is lengthened.[7]

In symmetrical high-spin ferric porphyrins, π spin density at the meso positions can result from interactions of the d_{xz} and d_{yz} metal orbitals with the π orbitals of e symmetry, the 3e π bonding or 4e π^* antibonding porphyrin MOs.[39,40] In chlorins and iBCs, this symmetry is lost. LaMar,[46] Strauss,[21,45] and their co-workers have noted that the HOMO in ferric chlorins ("a_{1u}") is symmetry and "energetically ideally situated" for π interactions with the iron d orbitals and concluded that the observed contact shifts in chlorins arise from π spin density from the "a_{1u}" orbital.

IEH calculations of the spin distributions for the HOMO and LUMO of **4**, based on the crystallographic coordinates described above, are shown in Figure 7. The HOMO spin profile is typical of "a_{1u}" hydroporphyrins; i.e., spin density is found at the α-carbons of all four pyrrole rings, with some density at the meso positions.[8,10]

If macrocycle to Fe π bonding occurs via the "a_{1u}" orbital, the meso protons of **4** should shift upfield because of the spin densities at those positions and at the flanking α-carbons. The experimentally observed chemical shifts of the meso protons follow the trend C5 > 20 ≈ 10 > 15 (Table III) and correspond to spin densities of 0.055, 0.042, 0.036, and 0.024 at C5, 20, 10, and 15,

(42) The crystallographic distances from the iron to the methylene and methyl carbons are as follows (Å): C21, 5.37; C23, 5.36; C25, 5.36; C27, 5.47; C29, 5.66; C31, 5.66; C33, 5.64; C35, 5.63; C22, 5.19; C24, 6.72; C26, 5.14; C28, 5.34; C30, 6.22; C32, 6.29; C34, 6.29; C36, 6.43. After inclusion of the hydrogens on each group, the Fe–H distances increase in the order CH_3 (pyrrolines) < CH_2 (pyrrolines) < CH_2 (pyrroles) ≈ CH_3 (pyrroles).

(43) Unpublished results.

(44) LaMar, G. N.; Eaton, G. R.; Holm, R. H.; Walker, F. A. *J. Am. Chem. Soc.* **1973**, *95*, 63.

(45) Pawlik, M. J.; Miller, P. K.; Sullivan, Jr. E. P.; Levstik, M. A.; Almond, D. A.; Strauss, S. H. *J. Am. Chem. Soc.* **1988**, *110*, 3007.

(46) Licoccia, S.; Chatfield, M. J.; LaMar, G. N.; Smith, K. M.; Mansfield, K. E.; Anderson, R. R. *J. Am. Chem. Soc.* **1989**, *111*, 6087.

(47) Balch, A. L.; LaMar, G. N.; Latos-Grazynski, L.; Renner, M. W. *Inorg. Chem.* **1985**, *24*, 2432.

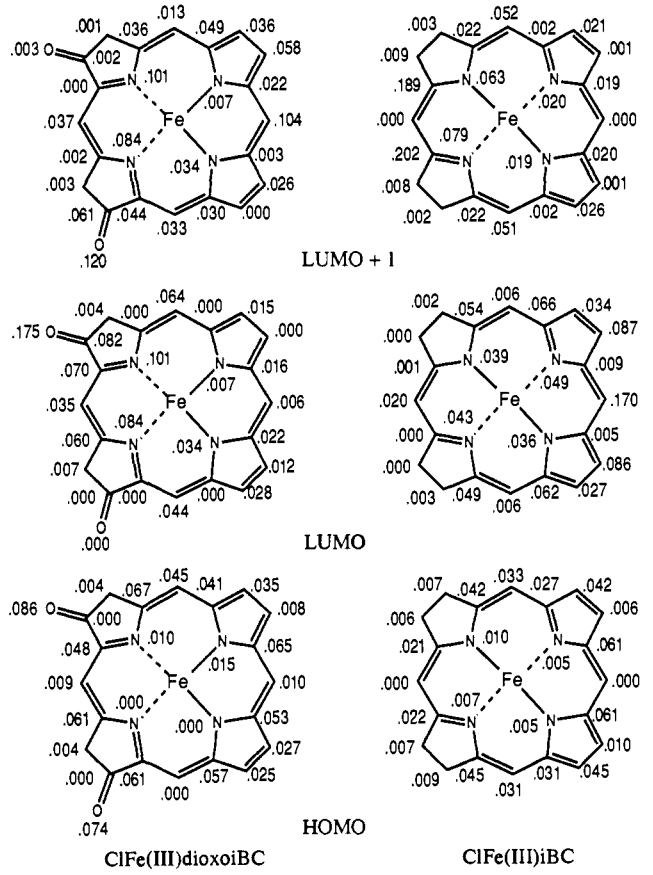

Figure 7. IEH calculations of the spin density profiles of the HOMOs, LUMOs, and LUMOs + 1 of **4** and $ClFe^{III}iBC$ (**6**). (All the ethyl groups were replaced by hydrogens in the computations.)

respectively. Thus, the calculated spin profile of the HOMO does not correctly predict the experimental order. Furthermore, the similarities between the NMR spectra of **4** and **6** at the meso positions require that the calculated spin profiles for the HOMOs of the two compounds be similar. The spin distribution in the HOMO of the $Fe^{III}OEiBC$ is shown in Figure 7. As expected for an iBC,[8,10] it is again "a_{1u}" but there are differences between the two compounds, particularly at the α- and meso-carbon regions of the pyrroline rings. It may perhaps be naive to expect exact agreement between the IEH calculations and the experimental results at the meso positions since the observed spin densities are all small (less than 0.06) and differ by not more than 0.03. As well, IEH calculations tend to overestimate the effects of heteroatoms: the keto groups in the present case.

Because Fe → π^* back-bonding is assumed to occur in iron(III) porphyrins, we have considered a similar possibility for **4**. The spin distribution for the LUMO of **4** is shown in Figure 7. The spin densities at C4, C5, and C6 vs those around C10, C15, and C20 might account for the observed meso proton shifts in **4**. However, given the constraints that the meso protons of **4** and **6** exhibit similar shifts, agreement with the calculated LUMO profile of the latter is very poor (Figure 7), particularly at C15 which is predicted to carry significant spin density (0.170). (We have confirmed the high-spin density predicted at C15 in the anion radical of H_2OEiBC.[43]) One last possibility is that the Fe in **6** (or **4**) interacts with the LUMO + 1. The spin distributions for the latter are included in Figure 7. Agreement with experiment is again not very good in either case. The basic conclusion to be reached from the above results is that the meso H NMR spectra of high-spin, pentacoordinate Fe(III) iBCs and dioxo-iBCs are remarkably insensitive to the presence of the peripheral keto groups, in spite of calculated differences in spin distributions for either the HOMOs or the LUMOs of the two compounds. (Note that the pyrroline rings differ more.)

What is unambiguously clear from the calculations (and the experimental redox potentials) is the large effect of the electro-

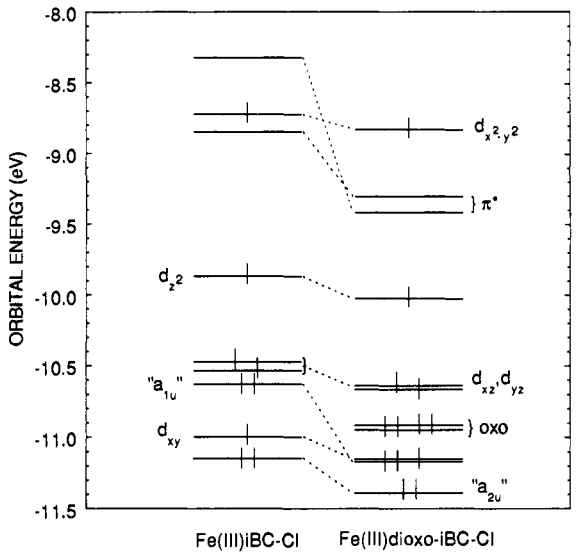

Figure 8. Energy level diagrams for **4** and **6**.

negative keto groups on the energy levels of dioxo-iBCs relative to analogous iBCs. Energy levels calculated for **4** and an equivalent iBC, in which each keto group has been replaced by two hydrogens, are shown in Figure 8. Both the HOMO and LUMO of **4** drop significantly; i.e., the molecule becomes harder to oxidize and easier to reduce. The consequences are clearly evident in the experimental redox potentials:[18] Both **3** and **4** are harder to oxidize by ~0.4 V than the corresponding iBCs. A similar shift is found for the reduction potential of **3**. The net effect of the dioxo groups is thus to *minimize* the redox characteristics of iBCs and render the porphyrindiones more akin to porphyrins. An additional feature of the dioxo compounds is the increased charge on the metal,[18] which is reflected in the potential of the Fe(II)/Fe(III) couple that is shifted to less negative values by ~0.2 V compared to either a porphyrin or an iBC. This difference in the charge on the iron should affect interactions with substrates, and the combined effects of the keto groups on the redox properties of the metal and the macrocycle may dictate the biological function of heme d_1. The biological use of keto groups to modulate redox properties is not limited to heme d_1. Chlorophylls[2] and Factor 430, the nickel tetrapyrrole found in methanogenic bacteria,[11] incorporate exocyclic rings with keto groups one carbon away from the macrocycle π systems. In all these cases, the redox potentials are also significantly shifted to more positive values.[15]

As has been observed in bacteriochlorophyll protein complexes,[48] the keto groups of heme d_1 may also be hydrogen bonded by nearby residues. Although such interactions are calculated[49] to have rather small effects on macrocycle redox potentials (<50 mV), they may anchor the prosthetic group within the apoprotein to optimize substrate interactions and electron transfer.[50]

Acknowledgment. This work was supported by the Division of Chemical Sciences, U.S. Department of Energy, under Contract DE-AC02-76CH00016 at BNL and by National Institutes of Health Grant GM36520 at MSU.

Supplementary Material Available: Listings of positional and anisotropic thermal parameters for the non-hydrogen atoms of **4** and **3**, bond distances and deviations from planarity in **3**, and stereoscopic packing diagrams of **4** and **3** (6 pages); listing of observed and calculated structure factors for **4** and **3** (28 pages). Ordering information is given on any current masthead page.

(48) Michel, H.; Epp, O.; Deinsenhofer, J. *EMBO J.* **1986**, *5*, 2445.
(49) Hanson, L. K.; Thompson, M. A.; Zerner, M. C.; Fajer, J. *The Photosynthetic Bacterial Reaction Center*; Breton, J., Vermeglio, A., Eds.; Plenum Press: New York, 1988; p 355.
(50) Forman, A.; Renner, M. W.; Fujita, E.; Barkigia, K. M.; Evans, M. C. W.; Smith, K. M.; Fajer, J. *Isr. J. Chem.* **1989**, *29*, 57.